Science Advances
AAAS

advances.sciencemag.org/cgi/content/full/6/49/eabd2508/DC1

Supplementary Materials for

Metachronal patterns in artificial cilia for low Reynolds number fluid propulsion

Edoardo Milana, Rongjing Zhang, Maria Rosaria Vetrano, Sam Peerlinck, Michael De Volder, Patrick R. Onck, Dominiek Reynaerts, Benjamin Gorissen*

*Corresponding author. Email: bgorissen@seas.harvard.edu

Published 2 December 2020, *Sci. Adv.* **6**, eabd2508 (2020)
DOI: 10.1126/sciadv.abd2508

The PDF file includes:

Other Supplementary Material for this manuscript includes the following:

(available at advances.sciencemag.org/cgi/content/full/6/49/eabd2508/DC1)

1. Hydraulic actuation

Pressurized air diffuses through the thin PDMS membranes of the actuator, resulting in the formation of tiny bubbles in the glycerol that perturb the fluid dynamic fields. In order to circumvent this issue, the actuators were filled with water and twelve pneumatic-hydraulic couplings were designed and manufactured to convert the pneumatic signal to a hydraulic signal. A schematic of the pneumatic-hydraulic couplings can be found in Fig. S1. Due to the slow actuation frequency, the higher inertia and viscosity of water than air is not reason of concerns.

2. Simulation and Experiment comparison

Although simulations explain very well the physics of the experimental observation, more insights can be provided about the differences in terms of quantitative results. As depicted in Fig. 3a and Fig. 5, flow velocities are reasonably within the same range between experiment and simulation (they depend on the cilia kinematics), while the integrated values show quantitative discrepancies. This happens due to the ideal assumptions required by the model as explained further. First of all, there are less data points in the measurements compared to simulation, leading to a loss of information. In fact, considering a single cycle, simulations have 500 data points and experiment only 20. This explains the differences observed in Fig. 3A, where some peaks in the fluid velocity might have been missed during the PIV. The loss of information is also related to some slight time shifts between simulation and experiment that can be observed in Fig. 3A. In that sense, it needs to be pointed out that the experimental data are more sensitive to eventual measurement errors. However, in our opinion, the most important mismatch originates from the assumptions on the cilia kinematics. Due to the absence of inertial effects, cilia kinematics are the only responsible of the fluid field generation. Indeed, while in the simulations the six cilia have identical kinematics, in the experiment this condition is only approximated. Even though we finely tuned the actuation of the six cilia to be as similar as possible, given the small scale there still were some misalignments, manufacturing imperfections and pressure drops in the fluidic circuit that may lead to stroke reductions. To quantify the kinematic mismatch we measured the swept areas of the six cilia from the PIV optical images and compared it with the assigned swept area of the simulations. The results are depicted in Fig. S9. The measurements are conducted for each cilium for four different beating cycles, where the error bars represent the standard deviation. Given the very small size of the cilia tips, the error bars are likely amplified by uncertainties in the measurements of the tip trajectories rather than real kinematics discrepancies between different cycles. However, it emerges how some cilia (4th and 5th) have reduced strokes compared to the others, altering the discussed ciliary obstruction mechanism and very likely being the cause of the experimental mismatches, particularly regarding the symplectic small phase shifts. Lastly, there is also the planar assumptions of the simulations. In the PIV we capture particles that, given the small size of the cilia diameter (1 mm), may be next to the cilia but not on the beating plane, therefore their net motion may be lower. To have an estimate of this last approximation, we run a simulation to calculate the flow field in the parallel plane placed at 1 mm distance from the beating plane. Indeed, we observe a 10% reduction of the net backflow velocity for the synchronous ciliary beating motion (Fig. S8).

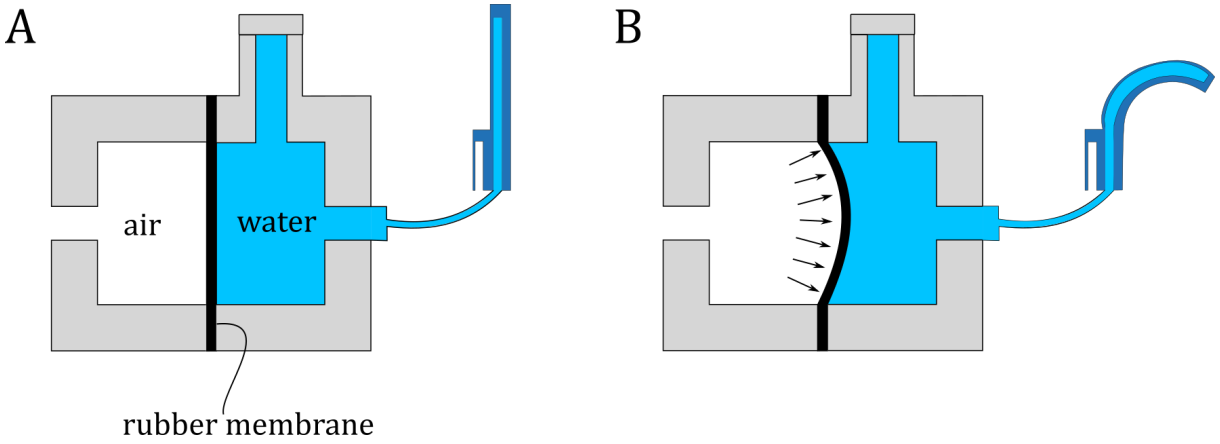

Fig. S1. Schematic overview of the pneumatic-hydraulic pressure converter. A) Coupling cross-section when the air chamber is at atmospheric pressure. B) When the air chamber is pressurized the membrane diplaces causing the actuation of the cilium's segment.

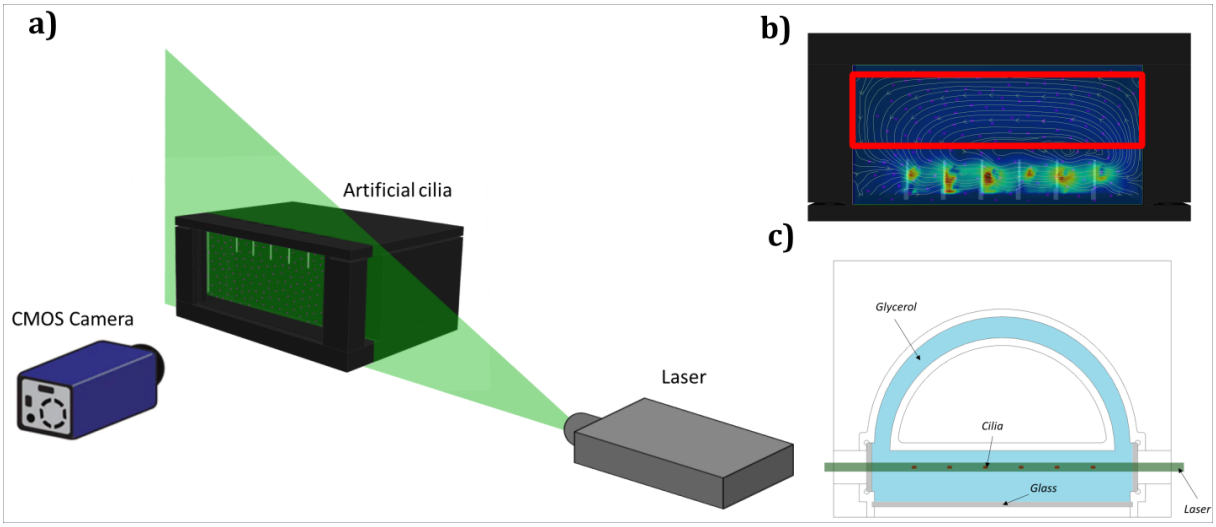

Fig. S2. PIV test setup to measure fluid flow. a) Sketch of the PIV experimental setup. b) Front view of the channel and measurement window. The red rectangle is the region where the backflow is calculated. c) Top view of the channel. Laser illuminates a portion of the fluid channel corresponding to the ciliary beating plane, approximating the 2-D simulations.

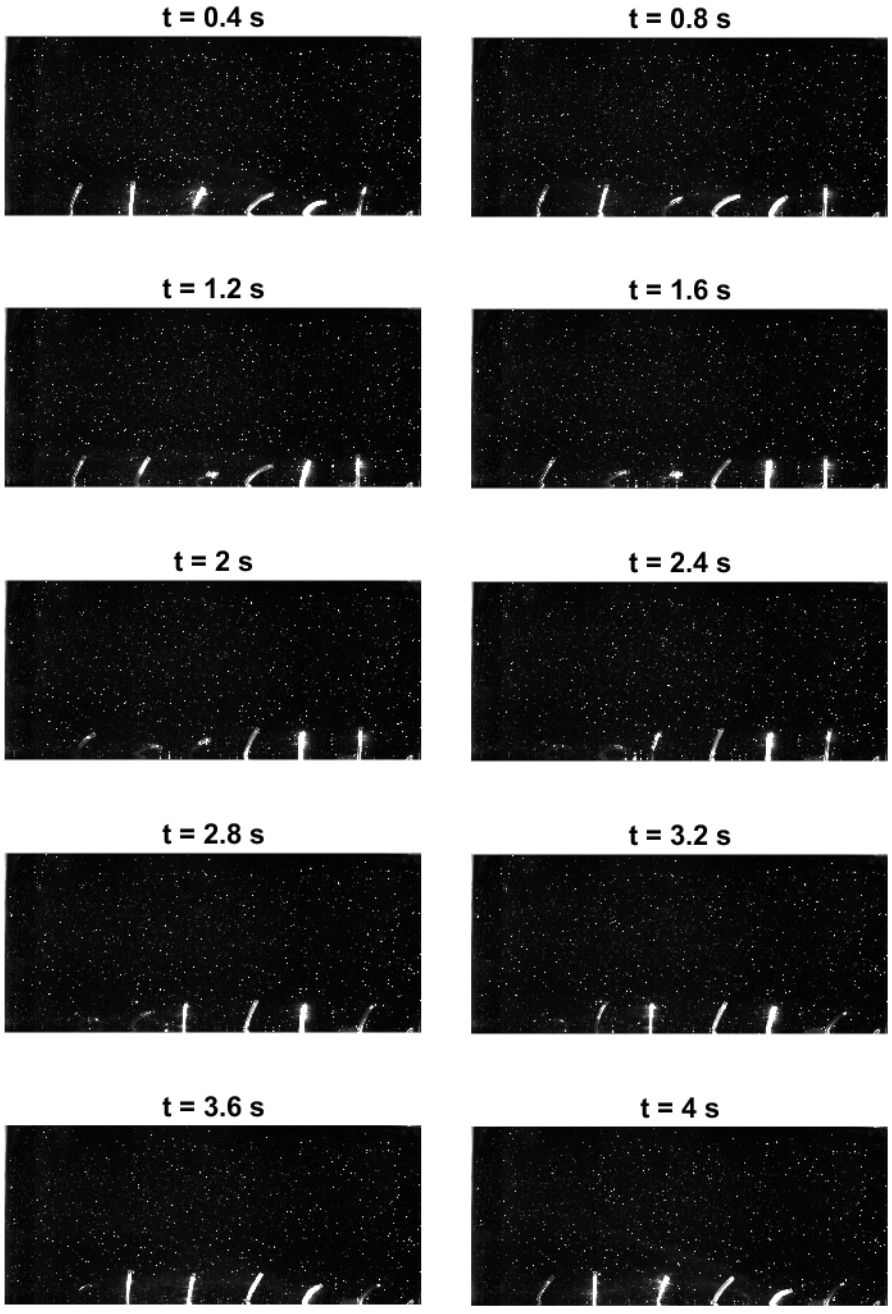

Fig. S3. PIV optical frames during one cycle of $\Delta\varphi = -\pi/3$.

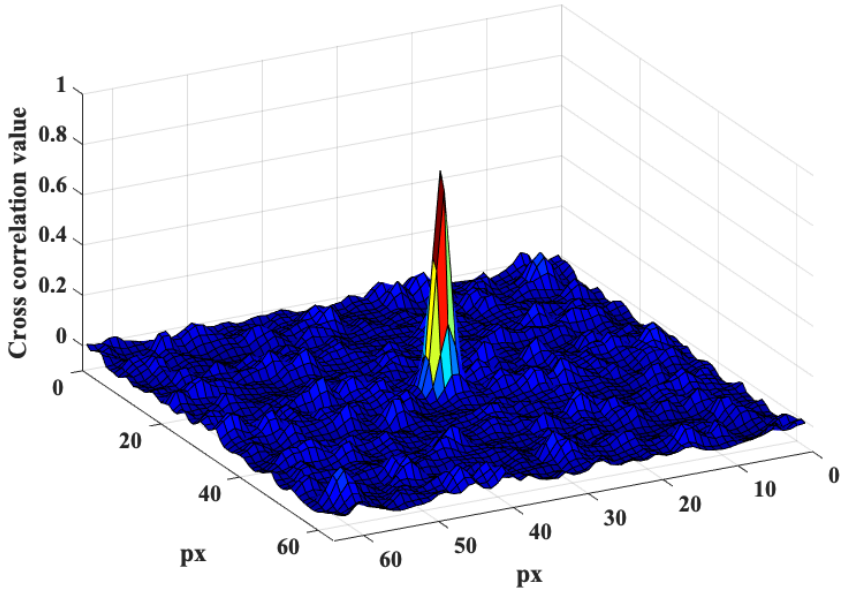

Fig. S4. Example of cross-correlation map obtained during the PIV processing.

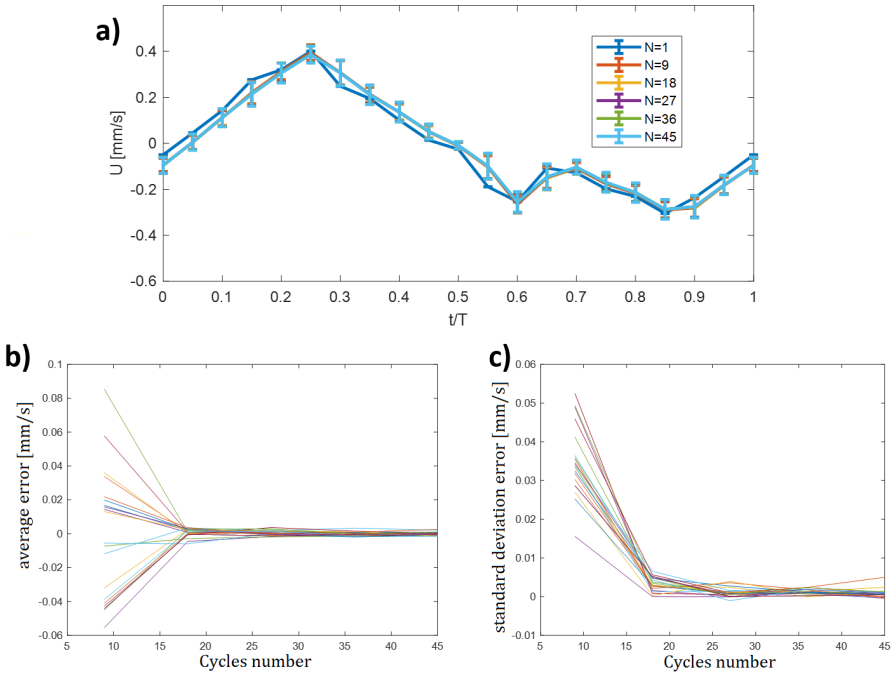

Fig. S5. Convergence of PIV measurements averaged over N cycles. a) N averaged backflow speed profile of the single cycle during a period $T = 4$s. b) Mean convergence and c) Standard deviation convergence. Each line corresponds to the velocity value at the same time in the cycle.

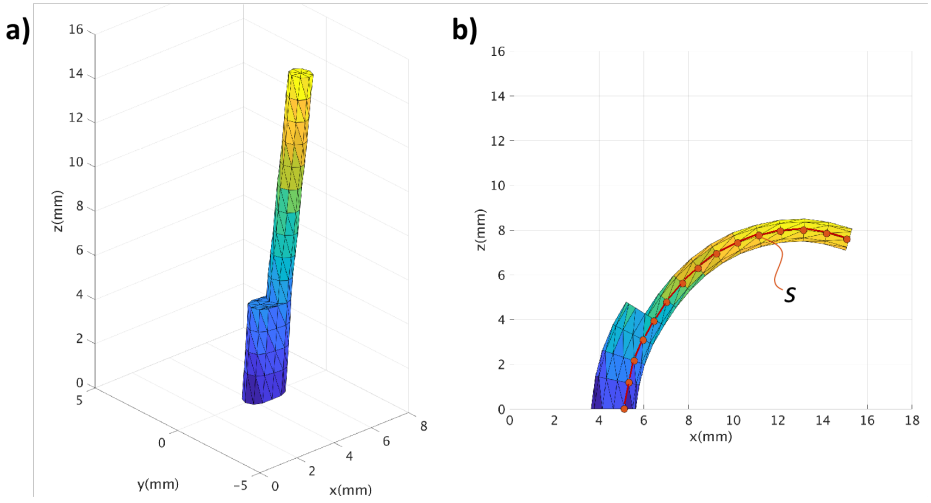

Fig. S6. The cilium surface is discretized using triangular surface elements. a) angle view. b) front view. The cilium centerline s is shown by the red line in b).

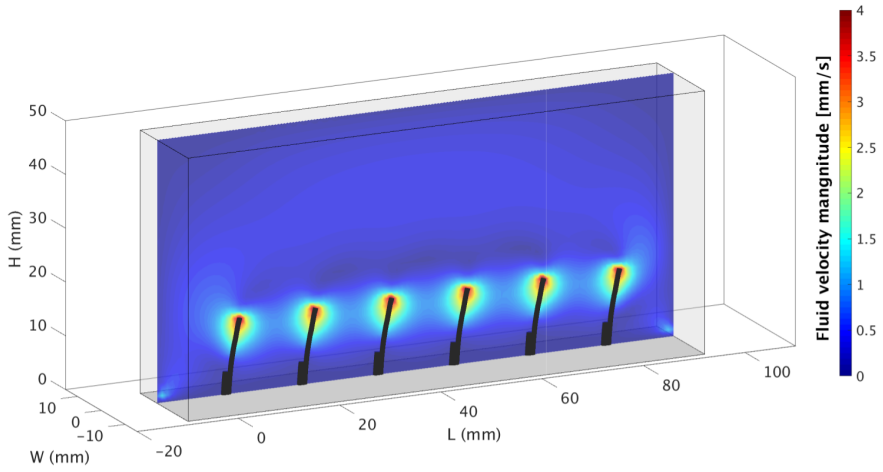

Fig. S7. Schematic view of the computational model. Snapshot of the CFD simulation for a single array of cilia for synchronous motion $\Delta\varphi = 0$. The contours represent the magnitude of the fluid velocity. The grey box represents the closed rectangular channel.

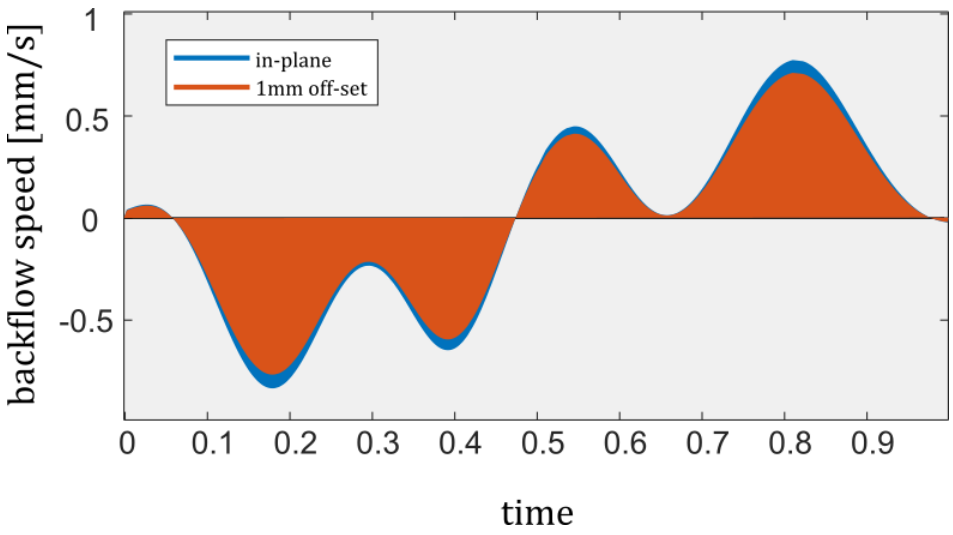

Fig. S8. Simulated backflow speed variation in the synchronous beating case between the beating plane ('in-plane') and a parallel plane that has a 1 mm off-set in the out-of-plane direction.

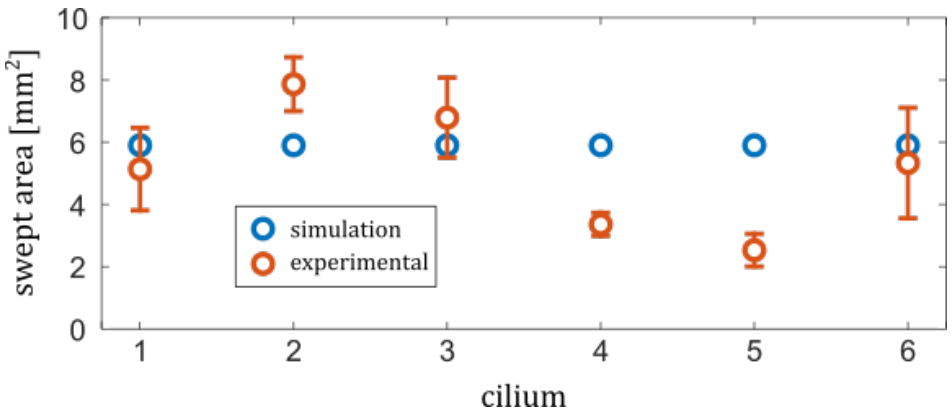

Fig. S9. Comparison between the simulated swept area (identical for the six cilia) and the experimentally measured swept areas. The measurements are conducted over 4 different cycles ($\Delta\varphi = -\pi/3$) and error bars correspond to the standard deviation.

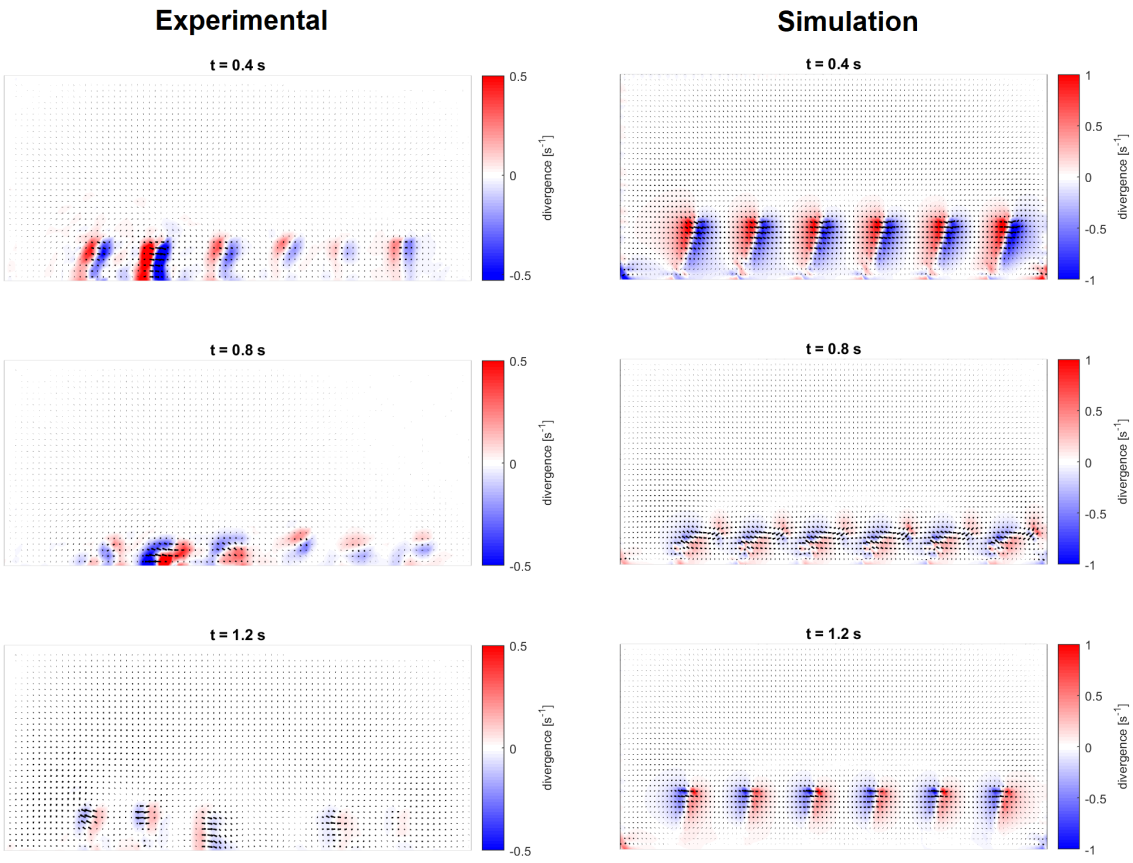

Fig. S10. Fluid field divergence for synchronous beating cilia at three different moments of the beating cycle.

Initial window size	64x64 pix^2
Final window size	24x24 pix^2
Windows overlap	50%
Cross-correlation peak ratio	3

Table S1. Processing parameters used to calculate the velocity map by Particle Image Velocimetry.

Movie S1. Metachronal actuation of artificial cilia This movie shows the different metachronal patterns of an array of six inflatable artificial cilia. Cilia are pneumatically actuated and move in air. Frames from this movie are displayed in Figure 1B